RESEARCH ARTICLE

Planar laser-induced fluorescence imaging in shock tube flows

J. Yoo · D. Mitchell · D. F. Davidson ·
R. K. Hanson

Abstract The planar laser-induced fluorescence (PLIF) imaging method was used to perform flow visualization and quantitative planar thermometry in shock tube flow fields using toluene as a fluorescence tracer in nitrogen. Fluorescence quantum yield values needed to quantify PLIF images were measured in a static cell at low pressures (<1 bar) for various toluene partial pressures in nitrogen bath gas. Images behind incident and reflected shocks were taken in the core flow away from regions affected by boundary layers. Temperature measurements from these images were successfully compared with predicted values using ideal shock equations. Measured temperatures ranged between 296 and 800 K and pressures between 0.15 and 1.5 atm. The average temperature discrepancies between measurements and the predicted values behind the incident and reflected shocks were 1.6 and 3.6%, respectively. Statistical analyses were also conducted to calculate the temperature measurement uncertainty as a function of image resolution. The technique was also applied to the study of more complex supersonic flows, specifically the interaction of a moving shock with a wedge. Measured temperatures agreed well with the results of numerical simulations in all inviscid regions, and all pertinent features of the single Mach reflection were resolved.

J. Yoo (✉) · D. F. Davidson · R. K. Hanson
High Temperature Gasdynamics Laboratory,
Department of Mechanical Engineering,
Stanford University, Stanford, CA 94305, USA
e-mail: jhyoo@stanford.edu

Present Address:
D. Mitchell
Department of Mechanical Engineering, Monash University,
Melbourne, Australia

1 Introduction

Planar laser-induced fluorescence (PLIF) is a non-intrusive optical detection scheme typically applied to monitor a trace species either seeded into or created within a flow field. The unique photo-physical properties of the tracer species combined with the selective and quantitative probing of this species with laser radiation offers the potential to measure key flow field parameters (e.g., species concentration, temperature, pressure, and density), and thereby provide a way to observe mixing and reaction chemistry, often in connection with combustion research (Kychakoff et al. 1984; Hanson 1986; Kohse-Höinghaus 2002; Wolfrum 1998). The PLIF signal S_T (photons collected per pixel) is expressed as the following equation:

$$S_T = \frac{E}{h\nu} n_T \sigma_T \phi_T AL \frac{\Omega}{4\pi} \bar{R}_{LIF} \qquad (1)$$

where E is the laser fluence in J/cm^2, $h\nu$ is the photon energy in J/photon, n_T is the tracer number density in cm^{-3}, σ_T is the absorption cross-section per molecule in cm^2, ϕ_T is the fluorescence quantum yield (FQY), AL is the probed volume in cm^3 per pixel, $\Omega/4\pi$ is the fractional collection solid angle, and R is the overall efficiency of the optics/camera components.

To date, the use of PLIF in shock tube studies has been limited. It has been used to image supersonic flow over a blunt body (McMillin et al. 1992) and shock-induced ignition (McMillin et al. 1990), and to quantitatively measure temperature in a transverse jet in a supersonic cross-flow (McMillin et al. 1993). Common PLIF tracers are acetone (Lozano et al. 1992), nitric oxide (Seitzman et al. 1985), OH (Seitzman et al. 1994), 3-pentanone (Neij et al. 1994), and toluene, but of these only NO and OH have been applied previously in studies of shock tube flows

to our knowledge. Initial interest in toluene as a tracer focused on its use in fuel/air ratio measurement in IC engines (Einecke et al. 2000), thermal stratification in an HCCI engine (Dec and Hwang 2009), oxygen and residual gas concentration measurement (Frieden et al. 2002) due to its strong quenching in the presence of oxygen, and demonstration of temperature imaging in heated turbulent free jet (Luong et al. 2006). Toluene compares quite favorably to ketones and other aromatics, as a tracer for performing quantitative thermometry, due to its very high sensitivity to temperature in the range of 300–900 K (Koban et al. 2004). One caveat is that due to the initial focus on use of toluene in engine environments, research has not been focused on its behavior at low pressures.

Despite relatively limited past use of toluene in the PLIF community until recently, its S_0–S_1 transition has been studied for over half a century (Burton and Noyes 1968). The photo-physical data such as absorption cross-section and FQY have all been measured in detail for a wide range of temperature and above atmospheric pressure conditions. Burton and Noyes (1968) first measured the absorption spectrum of the S_0–S_1 transition and found it to be very broad, extending from around 240 to 270 nm with a peak around 266.8 nm. The absorption cross-section at 248 nm (KrF laser) has been found to be insensitive to temperature between 300 and 850 K, with a value of approximately $3.1 \pm 0.2 \times 10^{-19} cm^2$ (Koban et al. 2004). The FQY of toluene, unlike its absorption cross-section, is very sensitive to temperature and has greater temperature sensitivity (by two orders of magnitude) than hydrocarbon-based tracers, such as acetone or 3-pentanone (Koban et al. 2004). The variation of FQY with temperature, relative to its value at 296 K and a pressure of 1 bar in N_2, for 248 nm excitation, has been empirically determined by Koban et al. (2004), The absolute value of FQY at the reference condition is estimated to be ≈ 0.09 for $\lambda_{ex} = 248$ nm, and 23 mbar of toluene (Burton and Noyes 1968).

Pressure also has a major influence on the FQY of toluene through its effect on the toluene vibrational relaxation rates in the upper electronic state. Collision-induced vibration energy transfer in toluene has been studied previously (Hippler et al. 1983; Toselli et al. 1991). Notably, non-radiative decay rate and FQY of benzene, a related compound of toluene, are known to increase and decrease, respectively, with the vibrational energy in the first excited singlet state (S_1), and toluene may be expected to have similar behavior (Hack and Langel 1980).

Using a static cell, a study was conducted to assess the relative FQY of toluene as a function of toluene partial pressure and total pressure, with results shown in Fig. 1. Laser fluence was set to 40 mJ/cm^2 within the static cell to preclude the effects of fluorescence signal saturation.
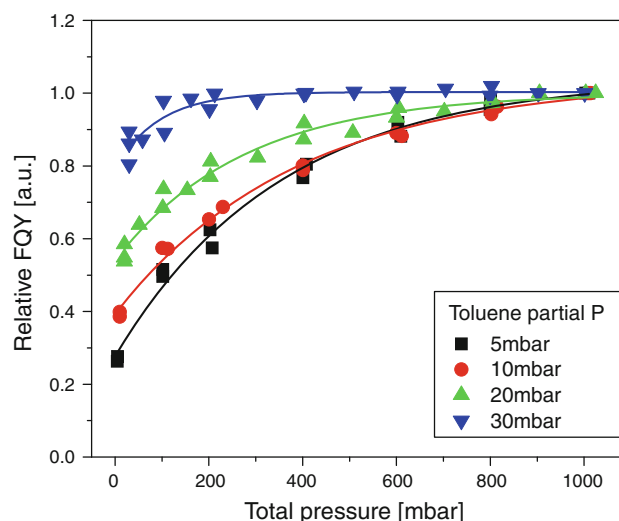

Fig. 1 Relative FQY for various partial pressure of toluene in N_2 bath gas, 296 K, and $\lambda_{ex} = 248$ nm. *Solid lines* are best numerical fit. The relative FQY values are normalized to the absolute FQY at 1 bar total pressure for each of the corresponding toluene partial pressures

The relative FQY values are defined as the absolute FQY values divided by the absolute FQY value at 1 bar total pressure and corresponding toluene partial pressure. Toluene FQY increases with increasing total pressure and toluene partial pressure. This variation must be considered when modeling fluorescence for toluene partial pressures and total pressures below about 50 and 1 bar, respectively.

A best numerical fit to the low pressure FQY data can be expressed by Eqs. 2 and 3, with the coefficients that are listed in Table 1. The relative FQY values (ϕ_{rel}) are used to scale the toluene FQY presented in (Koban et al. 2004) (Eq. 3), for conditions where toluene vibrational relaxation is incomplete (typically only in the pre-shock test gases in the current study).

$$\phi_{rel} = a - b \times c^{P_{total}} \quad (2)$$

$$\phi_{lowpressure} = \phi_{Koban}\phi_{rel} \quad (3)$$

Using toluene as a tracer, we have devised a PLIF strategy to quantitatively and sensitively measure temperature in compressible flow fields. Figure 2 demonstrates the strong

Table 1 Coefficients for low-pressure toluene relative FQY, for conditions of Fig. 1

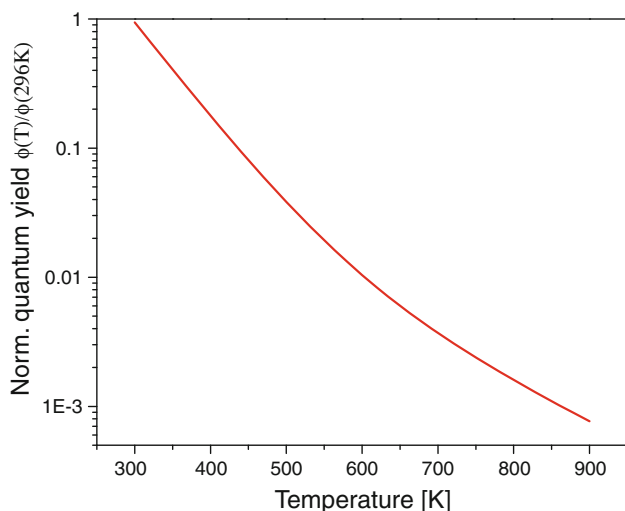| Toluene partial pressure (mbar)	a	b	c
5	1.04172	0.76536	0.99717
10	1.03523	0.64187	0.99743
20	1.00064	0.45983	0.99638
30	1.00314	0.20920	0.98949

Fig. 2 Toluene fluorescence quantum yield from Koban et al. (2004) at 248 nm excitation and 5–20 mbar toluene in 1 bar nitrogen

sensitivity of toluene FQY as a function of temperature at 248 nm as determined by Koban et al. (2004).

Highly uniform temperature fields for these studies were formed behind incident and reflected shock waves in a square cross-section shock tube that is capable of generating precisely known temperature and pressure conditions, with step changes across the shock waves. Images of incident and reflected shocks were first taken in regions of flow where wall effects were minimal (i.e. within the core of the flow) and well-described by the classical shock wave equations. Using the known photo-physical model of toluene given by Koban et al. (2004) and measured pressure and toluene concentration data, an algorithm was developed to convert PLIF signals into temperature. The measured temperature values were compared with theoretical values from the shock jump equations to validate the accuracy of this measurement technique. Statistical analyses of the images were also conducted to study the effects of noise as a function of binning of individual pixel signals.

The new PLIF method was then applied to image a more complex flow field: an incident shock wave propagating over a wedge. Here, PLIF imaging results can help in resolving current questions about the single Mach reflection, a region which is dominated by large pressure gradients, and for which no complete analytical solution exists.

2 Experimental setup

2.1 Aerosol shock tube

The experiments were performed in the aerosol shock tube (AST) in the High Temperature Gasdynamics Laboratory at Stanford University. A shock tube is a device in which uniform high temperature and pressure conditions can be readily generated by shock heating. The AST was built specifically to study the reaction kinetics of fuels with high molecular weight (and thus low vapor pressure); further details of the AST design can be found in (Hanson 2005; Haylett et al. 2009).

The AST, shown in Fig. 3, has a 3-m driver section with 15 cm internal diameter and a 9.6-m driven section with 11 cm diameter that transitions (over 30 cm) to a 2-m long recovery section, with square cross-section of 10 × 10 cm with rounded corners of $R = 1.8$ cm. At the end of the recovery section is a 15-cm transition to the test section with straight corners. The recovery sections gave the shock some distance to become stable after the transition.

The new test section was designed to facilitate the imaging of thermal and viscous boundary layers. The test section comprises $10 \times 10 \times 1.25$ cm^3 fused silica windows on three sides and a $10 \times 10 \times 2.5$ cm^3 window on the end wall. A picture of the test section is shown in Fig. 4.

This test section allows for imaging at any point within the flow. In addition, the design allows laser sheets to enter into the test section along multiple axes, through either one of the side, top, or end windows. One aluminum piece with pre-drilled holes was fitted in the place of the fourth side wall to accommodate pressure transducers.

Incident shock waves are generated by bursting polycarbonate diaphragms, which isolate the driven section, with high-pressure nitrogen. A simple operation schematic is shown in Fig. 5.

The stainless steel mixing assembly included a multivalve manifold with a magnetically driven stirring vane, both assemblies heated uniformly to approximately 330 K. Mixtures were made manometrically using capacitance manometers and pre-shock toluene concentrations in the shock tube (P_1) were confirmed using in situ 3.39-μm laser absorption (Klingbeil et al. 2007). Nitrogen was used with spectroscopic grade toluene with no further preparation

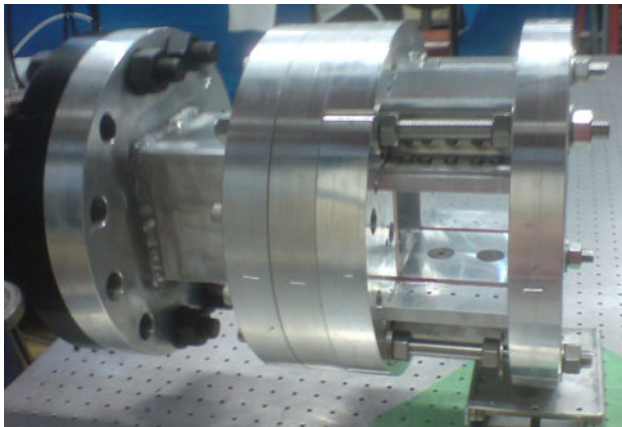**Fig. 3** Schematic of aerosol shock tube; overall length 18 m
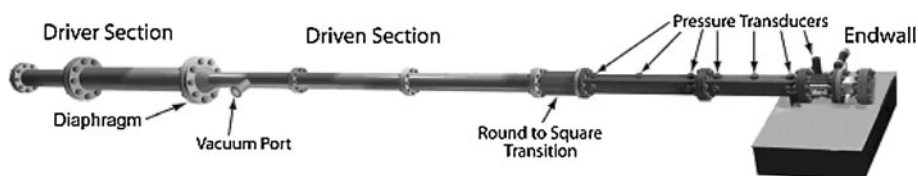
Fig. 4 Picture of the new shock tube test section designed for PLIF. The end wall is on the right side
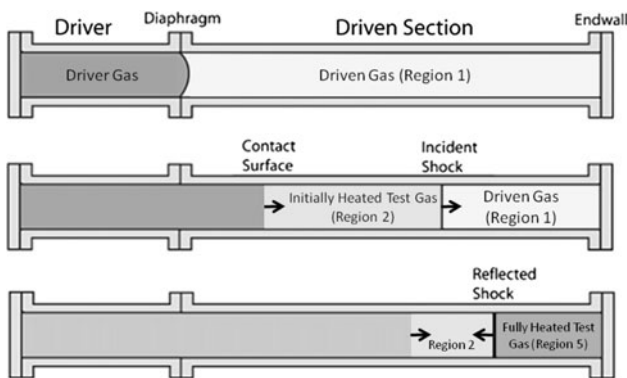

Fig. 5 Schematic of operation. The shock tube is filled with driven gas mixture. The incident shock then compresses and heats the driven gas. Upon reflection from the end wall, the reflected shock wave further compresses and heats the driven gas

except for vacuum pumping to remove dissolved volatiles and oxygen.

The setup is shown in Fig. 6. Different diaphragm thickness and initial pressure conditions were used to generate a wide range of conditions behind the incident and reflected shock waves. Shock images were taken in a region 3–9 cm from the end wall. The camera resolution employed was 0.06 mm/pixel for studies of both the core flow and flow over a wedge insert.

2.2 PLIF laser system

For PLIF measurements, a coherent KrF excimer (ComPEX pro 102) laser outputting pulses (20 ns) up to 250 mJ/pulse at 248 nm was used. This wavelength offers high-PLIF signal temperature sensitivity, while keeping the experimental setup relatively easy to configure.

Operation below the saturation limit of toluene fluorescence (i.e. linear response regime) was verified in situ
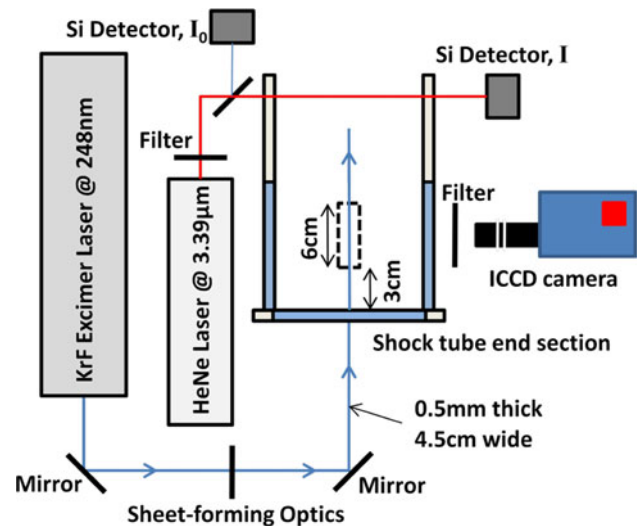

Fig. 6 Schematic of the shock tube/laser setup. In this configuration, the horizontal laser sheet enters through the end wall, and is imaged through the top window

for typical driven gas initial condition of 5% toluene in nitrogen at room temperature and 0.25 bar. In these experiments, the toluene PLIF signal was measured for laser fluencies of 40–150 mJ/cm^2. Fluorescence response was linear over the entire range of laser fluence (deviating <5% at the highest power). The laser sheet through the test section was 5-cm wide and 0.75-mm thick, and to prevent saturation, typical laser fluence in the test section was limited to 125 mJ/cm^2 or less.

In most cases presented here, the laser sheet enters the test section through the end wall window parallel to the floor of the shock tube to reduce the effects of laser sheet diffraction, which is caused when a collimated beam of light strikes the shock at grazing angles (Panda and Adamovsky 1995) leading to increased uncertainty in temperature measurement near the shock wave. However, when imaging the interaction of the incident shock with a wedge with the slant side facing upstream placed within the shock tube, the light sheet was introduced from a side window perpendicular to the wedge base to avoid laser sheet obstruction by the wedge. The pulse-to-pulse laser energy variation was monitored with a photodiode (LaVision).

Fluorescence signals were collected perpendicular to the laser sheet through the top window and focused with a 105 mm (focal length) f/4.5 achromatic UV lens (Nikon). The signal was imaged onto an intensified CCD camera (LaVision DynaMight, 1,024 × 1,024 pixels, 13 μm/pixel). A band-pass filter (bandwidth 20 nm, centered at 248 nm) was placed in front of the camera to suppress Rayleigh scattering and other scattered light. Images were recorded without hardware binning to maximize resolution. Images were subsequently processed using various binning

levels to maximize signal-to-noise ratio and to study the effects of noise as a function of hardware binning.

2.3 Image processing

Image processing requires taking the ratio of two PLIF images. The first, or reference, image, with PLIF signal $S_{296\,K}$, is an average of ten images where the pre-shock driven gas is stationary and at room temperature. This image is used to correct for laser sheet and optical/camera system variations. The second image, with PLIF signal S_T is a single-shot image of the flow region studied. Using the PLIF equation, and forming a ratio, we obtain.

$$\frac{S_T}{S_{296\,K}} = \frac{(\frac{E_T}{h\nu})n_T\sigma_T\phi_T\mathrm{AL}\frac{\Omega}{4\pi}\bar{R}_{\mathrm{LIF}}}{(\frac{E_{296\,K}}{h\nu})n_{296\,K}\sigma_{296\,K}\phi_{296\,K}\mathrm{AL}\frac{\Omega}{4\pi}\bar{R}_{\mathrm{LIF}}} \qquad (4)$$

Canceling common variables, the equation reduces to:

$$\frac{S_T}{S_{296K}} = \frac{E_T n_T \sigma_T \phi_T}{E_{296K} n_{296K} \sigma_{296K} \phi_{296K}} \qquad (5)$$

Several input parameters are required to solve Eq. 5. The fuel concentration, assumed homogeneous within the shock tube, and the initial pressure and temperature are known prior to the shock. Most importantly, post-shock flow field pressures are required to reduce Eq. 5 to a function of temperature. The pressure values are calculated from the measured shock speed using normal shock jump equations for both regions 2 and 5. Laser pulse energies (E_T and $E_{296\,K}$) are measured using a photodiode. Once all these parameters are considered, the equation is solved iteratively.

3 Results

3.1 Core flow images

Planar laser-induced fluorescence images taken in the core flow behind incident and reflected shocks were converted into temperature fields and compared with predicted temperature values. The comparison allows for an assessment of the accuracy and the validity of this measurement technique. A wide range of shock speeds and initial conditions were tested, with a resulting temperature range from 296 to 1,000 K. Example single-shot, full-frame images with measured and predicted temperature profiles for incident and reflected shock experiment are shown in Figs. 7 and 8, respectively. The two experiments were chosen to have different initial conditions and shock speeds to illustrate behavior over a wider range of temperatures. Axial and radial profiles in Figs. 7 and 8 are constructed by averaging temperature values across five pixels located at the centerline and 2 mm behind a shock wave, respectively.

Of note is that the temperature deviations in regions of higher temperature behind reflected shock are greater due to lower PLIF signals. The profiles exhibit uniform temperature distribution regardless of the orientation. The temperature profile in region 5 is less accurate than in regions 1 and 2 (i.e. a larger residual temperature is seen in Fig. 8) due to the lower toluene PLIF signal that occurs at higher temperatures.

The signal-to-noise ratio (SNR) of PLIF images as a function of binning level was also studied, and is shown in
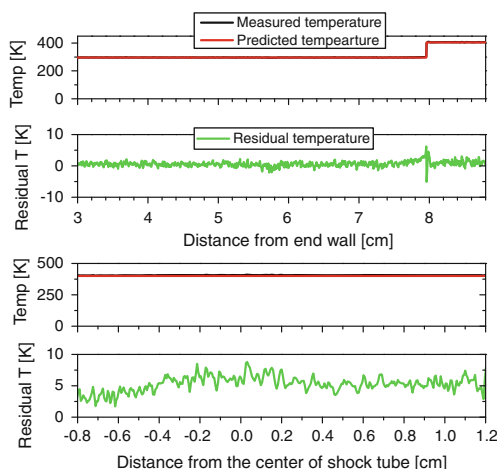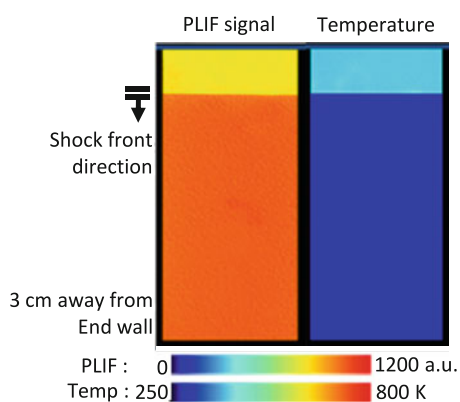

Fig. 7 Incident shock wave measurements. Example (*left*) corrected PLIF intensity and temperature images. Initial conditions: $P_1 = 0.067$ bar, $X_{tol} = 3.8\%$, $T_1 = 296$ K, $V_s = 546$ m/s, incident shock attenuation = 1.3% per m. *Downward-pointing arrow*: direction of incident shock. Temperature and residual temperature (*right*)

(between measured and predicted) profiles in the core flow. *Upper plots*: axial orientation along the central column of pixels (averaged across 5 pixels width); *lower plots*: radial orientation, along the row of pixels 2 mm behind incident shocks; a flat temperature distribution across the laser sheet is evident
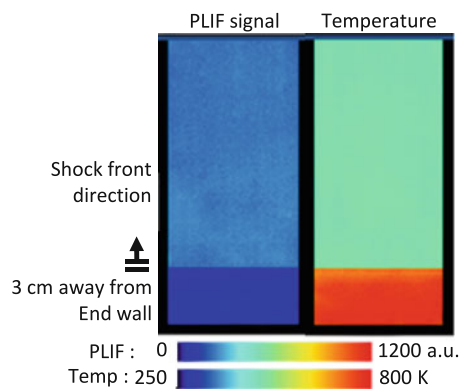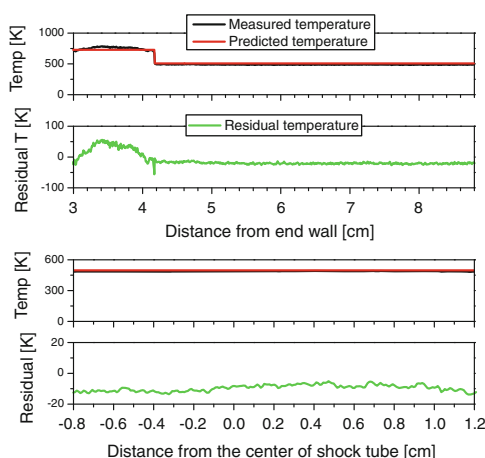
Fig. 8 Reflected shock wave measurements. Example (*left*) corrected PLIF intensity and temperature images. Initial conditions: $P_1 = 0.031$ bar, $X_{tol} = 4.5\%$, $T_1 = 296$ K, $V_s = 723$ m/s, incident shock attenuation = 1.5% per m. *Upward-pointing arrow*: direction of reflected shock wave. Temperature and residual temperature (*right*)

(between measured and predicted) profiles in the core flow. *Upper plots*: axial orientation along the central column of pixels (averaged across 5 pixels width); *lower plots*: radial orientation, along the row of pixels 2 mm behind reflected shocks; a flat temperature distribution across the laser sheet is evident
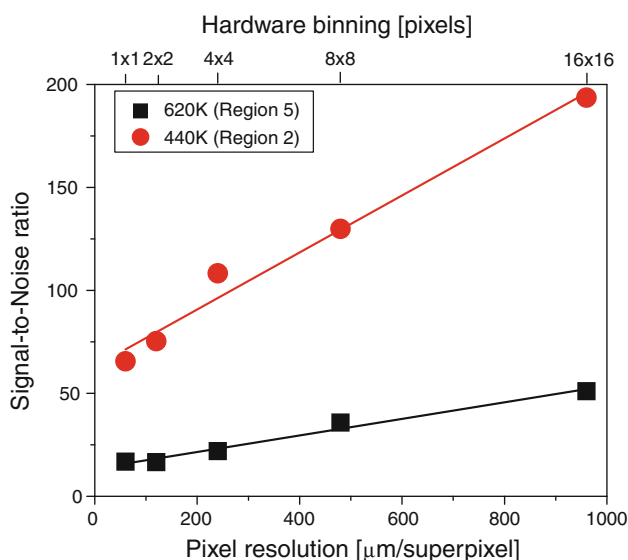

Fig. 9 SNR as a function of pixel resolution using hardware binning. Toluene mole fraction, X_{tol}, for both temperatures were fixed at 0.9%

Fig. 9. In the case of shot-noise-limited behavior, SNR should increase as binning level increases, while image resolution decreases. For this study, the spatial resolution in the images, with no hardware binning was 0.06 mm/pixel, and reduced to 1 mm/pixel at the maximum binning (16 × 16 pixels). For high-temperature applications where low PLIF signals are expected or when trying to image small-scale flow features, an optimum balance of SNR and image resolution is required.

Approximately, 50 incident and reflected shock single-shot images were taken to assess the variation of measurement

accuracy with temperature. Images were taken without hardware binning to maximize pixel resolution. The temperature values were then averaged (binned) from a 5 × 5 pixel square 2 mm behind their respective shocks. For the current set of data, shock attenuation was neglected due to its negligible effect on temperature. A plot of predicted versus measured temperature is presented in Fig. 10.

Near room temperatures, the mean measurement difference is within 0.4%. However, as temperature increases the mean difference increases to about 1.6% for regions behind the incident shock and 3.6% for regions behind the reflected shock. This increased error may be attributed to the decrease in PLIF signal with temperature as well as uncertainty in the absorption cross-section and relative FQY models (6 and 10%, respectively).

3.2 Flow over a wedge

Having demonstrated the accuracy of the PLIF-toluene technique in the core flow region where temperature can be predicted with confidence, we applied this technique to a more complex flow field: an incident shock wave propagating up a wedge (see Fig. 11).

Although the flow cannot be completely predicted analytically with existing theory, flow features, such as the Mach stem and slipstream region in the reflected shock are clearly distinguishable in Fig. 12. The aluminum wedge is 5-cm wide and 7.5-cm long with an angle of 30°. The base of the wedge is fixed, parallel to a side wall, with two columns (2.5-cm long). The back end of the wedge is about 1 cm from the end wall. The columns were designed to not interfere with flow patterns over the wedge. The laser sheet
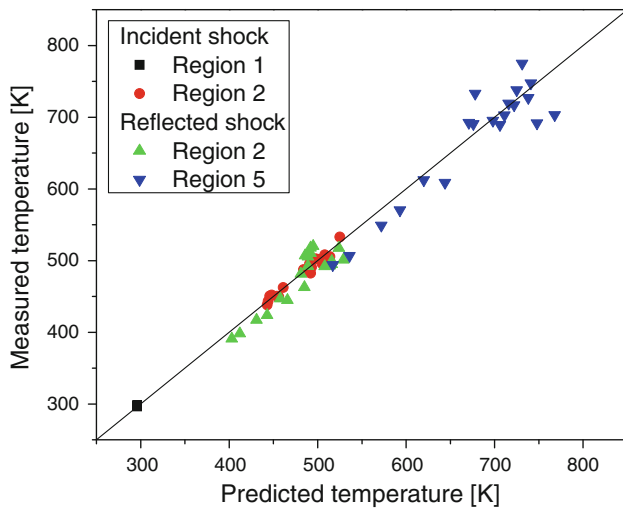
Fig. 10 Comparison of measured and predicted temperature in the core flow. Single-shot images were taken at full resolution without hardware binning, about 3–9 cm away from the end wall
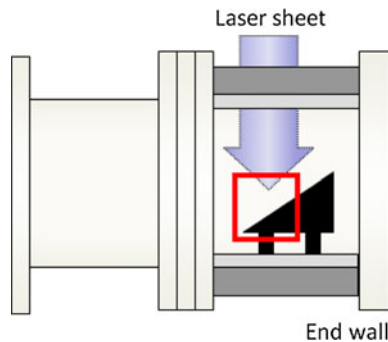

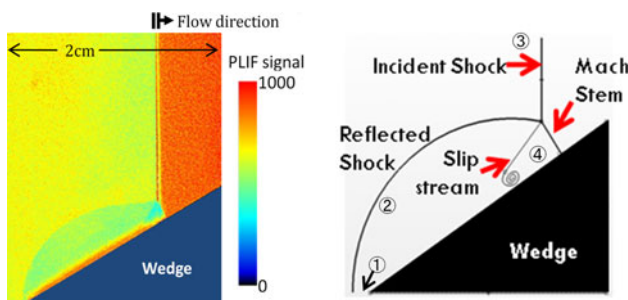Fig. 11 Location of the wedge in the test section. Flange configuration identical to Fig. 5

Fig. 12 PLIF signal image (*left*) of an incident shock traveling over a wedge. Single Mach reflection is visible as well as the diffraction effect in the incident shock wave transition when laser is introduced through the side window; (*right*) schematic of a single Mach reflection (Ben-Dor 2007)

enters the test section via the side window, since the placement of the wedge itself precludes entry via the end window. The PLIF signal is observed through the top window. The beam must be carefully aligned (so that it
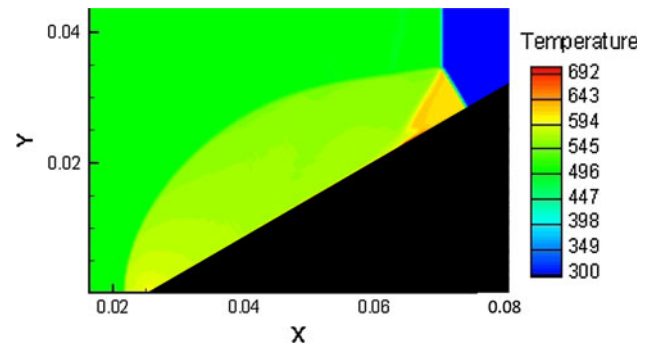

Fig. 13 Temperature field simulated using Fluent 6.0

does not enter the test section at a grazing angle) to minimize the effects of laser sheet diffraction at the incident shock front. The wedge surface was coated with black matte spray paint to minimize scatter. The characteristic features of a single Mach reflection are clearly visible. The structures evident in the image are in agreement with those predicted by theory. However, the pressure field needed to convert the images to temperature inside the reflected shock region cannot be analytically predicted. A commercial CFD package, Fluent 6.0, was used to simulate temperature and pressure fields thereby providing a numerical model for quantitative comparison. A coupled density solver was used to solve the continuity equation in control volume form. The ratio of specific heat for toluene and nitrogen was expressed as third-order polynomials, and viscosity was treated via the Menter Shear Stress Transport (SST) model (Menter 1994). Third-order AUSM (Advection Upstream Splitting Method) flux splitting was used for discretization (Liou and Steffen 1993), and an explicit solver was used. The resultant temperature field after the incident shock reaches the leading edge of the wedge can be seen in Fig. 13. An image of the synthetic PLIF signal can be constructed using the calculated temperature, pressure, and mole fraction results from CFD along with the toluene photo-physical models (Koban et al. 2004 and Eq. 2). This image is shown in Fig. 14 next to the experimental PLIF image with matching initial conditions. The experimental and synthetic PLIF signal values for various regions of the flow are listed in Table 2. The values match extremely well except within the slipstream region. It should be emphasized that a 5% discrepancy in PLIF signal at these pressures corresponds to only 0.5% variation in temperature. The reason for the discrepancy in the slipstream region is uncertain; however it should be noted that this is the only region in which viscous terms are important, so it may simply be that the Fluent simulation was not capable of capturing the necessary non-ideal flow physics in that region. However, the excellent performance in all inviscid regions is promising. Further studies of this generic flow using the PLIF diagnostic are planned.
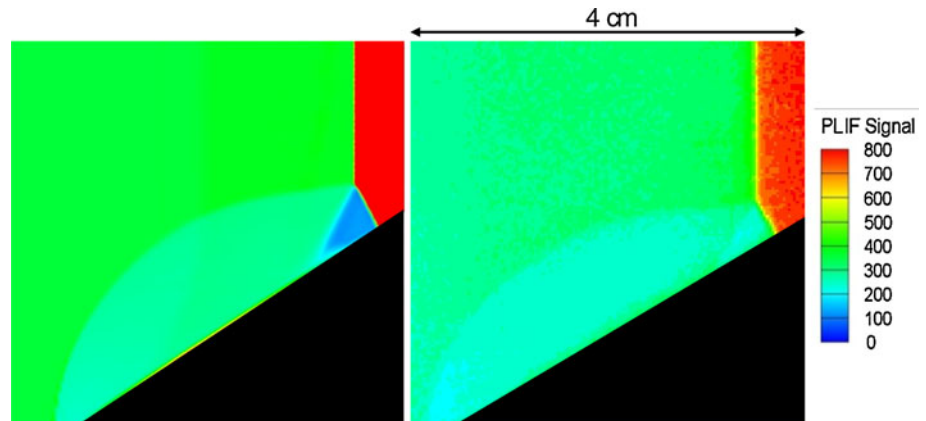
Table 2 Comparison of the actual and synthetic PLIF signal values
for various regions of the flow

	Regions	Actual PLIF signal level	Synthetic PLIF signal level
1	Bow shock at nose	260	250
2	Reflected shock	280	275
3	Free stream	375	365
4	Slip stream	310	135

The regions are labeled in Fig. 12

3.3 Future plans

Planar laser-induced fluorescence imaging with a toluene
tracer can provide accurate 2-D temperature field mea-
surements for shock tube flows with known pressure and
known or uniform mole fraction. In the future, experi-
ments are planned to image regions near the side and end
walls to characterize the viscous and thermal boundary
layers and the bifurcation of the reflected shock. Other
plans include study of the temperature field generated by
shock reflection from a curved or notched end wall. Other
potential extensions to the technique include the use of
multiple wavelengths to explicitly determine pressure and
temperature.

4 Conclusions

A quantitative temperature-field measurement technique
based on toluene PLIF, allows sensitive visualization of
temperature in shock tube flow fields. Toluene was selected
as the tracer due to its high-temperature sensitivity. Addi-
tional low-pressure toluene FQY data were measured as a
complement to the existing toluene FQY database. The
changes in SNR as a function of binning level were also
studied. Images of incident and reflected shocks were taken
in uniform flow conditions to characterize the accuracy of
the measurement technique. The mean accuracy ranges
from 0.4% to 3.6% within the range 296–800 K. Toluene
provides high-temperature sensitivity up to 800 K. For
higher temperatures, other tracers, such as NO may be
more appropriate. The same technique was then applied to
study shock interaction with a wedge. The overall structure
of the observed single Mach reflection agreed well with
shock reflection theory. Detailed structure was examined
by comparison with a synthetic PLIF image generated
using a commercial CFD package. The results in all
inviscid regions agreed very well with the simulation, some
discrepancy was seen in the model predictions of the vis-
cous slipstream region. Further measurements using this
new sensitive toluene PLIF imaging method are planned to
study this region and test current theoretical models of the
viscous slipstream flow. Furthermore, this diagnostic may
be applicable to investigations of the NTC (negative tem-
perature coefficient) regime, where ignition chemistry at
temperatures less than 900 K is of interest to the com-
bustion community.

References

Ben-Dor G (2007) Shock wave reflection phenomena. Springer,
    Heidelberg
Burton CS, Noyes JWA (1968) Electronic energy relaxation in
    toluene vapor. J Chem Phys 49:1705–1714
Dec JE, Hwang W (2009) Characterizing the development of thermal
    stratification in an HCCI engine using planar-imaging thermom-
    etry. SAE Int J Eng 2(1):421–438

Einecke S, Schulz C, Sick V (2000) Measurement of temperature, fuel concentration and equivalence ratio fields using tracer LIF in IC engine combustion. Appl Phys B 71(5):717–723

Frieden D, Sick V, Gronki J, Schulz C (2002) Quantitative oxygen imaging in an engine. Appl Phys B 75:137–141

Hack W, Langel W (1980) KrF-laser-induced fluorescence of benzene and its fluorinated derivates in the gas phase. Il Nuovo Cimento B 63(1):207–220

Hanson T (2005) The development of a facility and diagnostics for studying shock-induced behavior in micron-sized aerosols. Mech Eng Stanford Univ

Hanson RK (1986) Combustion diagnostics: planar flowfield imaging. In: 21st Symposium (international) on Combustion. The Combustion Institute, p 1677–1691

Haylett DR, Lappas PP, Davidson DF, Hanson RK (2009) Application of an aerosol shock tube to the measurement of diesel ignition delay times. Proc Combust Inst 32:477–484

Hippler H, Troe J, Wendelken HJ (1983) Collision deactivation of vibrationally highly excited polyatomic molecules, II. Direct observations for excited toluene. J Chem Phys 78:6709–6717

Klingbeil AE, Jeffries JB, Hanson RK (2007) Temperature-dependent mid-IR absorption spectra of gaseous hydrocarbons. J Quant Spectrosc Radiat Transf 107:407–420

Koban W, Koch JD, Hanson RK, Schulz C (2004) Absorption and fluorescence of toluene vapor at elevated temperatures. Phys Chem Chem Phys 6(11):2940–2945

Kohse-Höinghaus K, Jeffries JB (2002) Applied combustion diagnostics. Taylor & Francis, London

Kychakoff G, Howe RD, Hanson RK (1984) Quantitative flow visualization technique for measurements in combustion gases. Appl Opt 23(5):704–712

Liou M-S, Steffen CJ (1993) A new flux splitting scheme. J Comput Phys 107(1):23–29

Lozano A, Yip B, Hanson RK (1992) Acetone: a tracer for concentration measurements in gaseous flows by planar laser-induced fluorescence. Exp Fluids 13(6):369–376

Luong M, Koban W, Schulz C (2006) Novel strategies for imaging temperature distribution using toluene LIF. J Phys Conf Ser 45:133–139

McMillin BK, Lee MP, Paul H, Hanson RK (1990) Planar laser-induced fluorescence imaging of shock-induced ignition, in 23rd symposium (International) on combustion. The Combustion Institute, pp 1909–1913

McMillin BK, Lee MP, Hanson RK (1992) Planar laser-induced fluorescence imaging of shock-tube flows with vibrational nonequilibrium. AIAA 30:436–443

McMillin BK, Palmer JL, Hanson RK (1993) Temporally resolved, two-line fluorescence imaging of NO temperature in a transverse jet in a supersonic cross flow. Appl Opt 32(36):7532–7545

Menter FR (1994) Two-equation eddy-viscosity turbulence models for engineering application. AIAA J 32(8):1598–1605

Neij H, Johansson B, Alden M (1994) Development and demonstration of 2D-LIF for studies of mixture preparation in SI engines. Combust Flame 99(2):449–457

Panda J, Adamovsky G (1995) Laser light scattering by shock waves. Phys Fluids 7:2271–2279

Seitzman JM, Kychakoff G, Hanson RK (1985) Instantaneous temperature field measurements using planar laser-induced fluorescence. Opt Lett 10(9):439–441

Seitzman JM, Hanson RK, DeBarber PA, Hess CF (1994) Application of quantitative two-line OH planar laser-induced fluorescence for temporally resolved planar thermometry in reacting flows. Appl Opt 33(18):4000–4012

Toselli BM, Brenner JD, Yerram ML, Chin WE, Ding KD, Barker JR (1991) Vibrational relaxation of highly excited toluene. J Chem Phys 95(1):176–188

Wolfrum J (1998) Lasers in combustion: from basic theory to practical devices. Proc Comb Inst 27:1–41